Mon. Not. R. Astron. Soc. **000**, 1–11 (1998) Printed 1 February 2008 (MN LATEX style file v1.4)

Principal Component Analysis of Synthetic Galaxy Spectra

Shai Ronen, Alfonso Aragón-Salamanca, Ofer Lahav
Institute of Astronomy, The Observatories, Madingley Road, Cambridge, CB3 OHA

Submitted to MNRAS, 8 May 1998

arXiv:astro-ph/9805130v1 11 May 1998

ABSTRACT

We analyse synthetic galaxy spectra from the evolutionary models of Bruzual & Charlot and Fioc & Rocca-Volmerange using the method of Principal Component Analysis (PCA). We explore synthetic spectra with different ages, star formation histories and metalicities, and identify the Principal Components (PCs) of variance in the spectra due to these different model parameters. The PCA provides a more objective and informative alternative to diagnostics by individual spectral lines. We discuss how the PCs can be used to estimate the input model parameters and explore the impact of noise in this inverse problem. We also discuss how changing the sampling of the ages and other model parameters affects the resulting PCs. Our first two synthetic PCs agree with a similar analysis on observed spectra obtained by Kennicutt and the 2dF redshift survey. We conclude that with a good enough signal-to-noise ($S/N \gg 10$) it is possible to derive age, star formation history and metallicity from observed galaxy spectra using PCA.

Key words: methods: data analysis – galaxies: evolution – galaxies: fundamental parameters – galaxies: stellar content.

1 INTRODUCTION

Present and future galaxy surveys will provide large numbers of spectra, which will allow the determination of many properties of different galaxy populations. For example, the Anglo-Australian Observatory 2-degree-Field (2dF) Galaxy Survey aims to collect 250,000 spectra and is already gathering data (e.g. Colless 1998). The Sloan Digital Sky Survey (e.g. Gunn & Weinberg 1995; Fukugita 1998) will observe the spectra of millions of galaxies. Such large data sets will provide a wealth of information, pertaining to the distribution and properties for a vast variety of galaxy types. The analysis and full exploitation of such data sets will require well understood, automated and objective techniques to extract as much information as possible on the evolutionary properties of the galaxies. In this paper we present the method of Principal Component Analysis (PCA) to extract such information by looking at the underlying parameters that determine each galaxy spectrum. We apply the method to synthetic galaxy spectra generated using the evolutionary population synthesis technique (see, e.g., Bruzual & Charlot 1993; Fioc & Rocca-Volmerange 1997). For such model spectra, the evolutionary properties are known *a priori*, allowing us to relate the information provided by the PCA to the input model parameters.

Three of the most important parameters which determine a galaxy spectrum are age, star formation history and metallicity. Given a spectrum, one would like to deduce these parameters. This can be done in principle by comparing the given spectrum with synthetic spectra based on models of stellar evolution. Attempts have been made in this direction using template fitting. Summarising these attempts, Nobuo Arimoto (in Leitherer et al. 1996) writes that 'It turns out that the present-day population synthesis models cannot derive age and metallicity of stellar populations, independently, from the photo-spectroscopic features of elliptical galaxies'. We note, however, that improvement in the statistical analysis technique may also help, and methods more sophisticated than simple template fitting are available.

In this paper we explore a standard statistical technique, Principal Component Analysis, as a promising approach which may prove better than template fitting. PCA has previously been applied to data compressing and classification of spectral data of stars (e.g. Murtagh & Heck 1987; Bailer-Jones et al. 1997), QSO (e.g. Francis et al. 1992) and galaxies (e.g. Connoly et al. 1995; Folkes, Lahav & Maddox 1996; Sodre & Cuevas 1997; Galaz & de Lapparent, 1997; Bromley et al. 1998; Glazebrook, Offer & Deeley 1998). Here we apply it to samples of synthetic spectra in the 3650–7100Å rest-frame wavelength range (similar to that of the 2dF and Sloan surveys) to get physical insight into the way different parameters affect the spectrum of a galaxy. We leave the comparison with observations to a future paper. However we already notice an encouraging good resemblance

© 1998 RAS

between the PCs that we get from the synthetic spectra and those one gets from Kennicutt's (1992) data of field galaxies.

The organisation of the rest of this paper is as follows. In section 2 we describe the synthetic models we have used. In section 3 we present the PCA method. In section 4 we analyse a sample of instantaneous burst galaxy models with different ages, find the first Principal Components (PCs), discuss their physical significance, their use to determine the age, and how different age sampling affects the resulting PCs. In section 5 we explore galaxy models with different ages and different star formation histories, and discuss how PCA may enable us to discriminate between the effect of these two parameters on the spectra. In section 6 we quantify the effect of varying metallicity on the spectra. In section 7, we check how noise in the data may affect the discriminatory power of our method. We end with a discussion and the conclusions of our investigation.

2 THE SYNTHETIC MODELS

We have chosen to use two different synthetic models from different authors so that we can assess how model-dependent our conclusions are. The first one is PEGASE (Projet d'Etude des GAlaxies par Synthèse Evolutive), by Fioc & Rocca-Volmerange (1997). The second one is the isochrone synthesis model of Bruzual & Charlot (1996 —GISSEL: Galaxy Isochrone Synthesis Spectral Evolution Library). Given a Star Formation Rate history, an Initial Mass Function and metallicity (only solar metallicity for PEGASE), these models provide galaxy spectra as a function of age. We used these models to simulate spectra in the optical range $\lambda\lambda$3650–7100Å, appropriate for the 2dF and Sloan surveys.

The PEGASE model extends from the UV to the NIR and is based on a combination of observational and synthetic libraries of stellar spectra. The optical range in which we are interested is based on the library of Gunn & Stryker (1983), and has 10Å spectral bins. One advantage of this model is that, on top of including the contribution to the spectra of the stellar population, it also calculates the intensities of Nebular emission lines. Since the shape of the emission lines is not specified, for the purpose of this paper we simulated the shape of all emission lines as a Gaussian with a sigma of 10 angstroms, i.e., implying a spectral resolution comparable to that of the stellar component in the models. At such resolution, the emission lines will be unresolved for normal galaxy spectra (i.e., not AGNs), thus the shape and width of the lines would be determined by the instrumental resolution. The origin of the nebular emission lines is the absorption of Lyman continuum photons below 912Å by the gas, which gets ionised, and reaches recombination equilibrium (cf. Osterbrock 1989). We let the fraction of absorbed photons to be 0.7 in all our simulations *.

The Bruzual & Charlot (1996; BC) isochrone model of stellar population synthesis is widely used in the interpretation of observed galaxy spectra. In the optical range, and for solar metallicity stellar populations, it offers a choice between three stellar libraries. We have confirmed that both PEGASE and BC models give very similar spectra when both are used to simulate populations of different ages based on the same stellar library (e.g., Gunn & Stryker 1983), and with no emission lines. The disadvantage of the BC model is that it does not provide emission lines. However the last version of the BC models have the advantage of providing spectra for different metalicities. These are based on the theoretical stellar spectra compiled by Lejeune, Cuisinier & Buser (1996). We therefore chose this model for exploring the impact of different metalicities on the spectra using PCA.

In both models we used the Initial Mass Function (IMF) of Scalo (1986), which is representative of the solar neighbourhood.

Note that we have not included the effects of interstellar reddening in the models for simplicity, since the main aim of this paper is to illustrate the PCA technique. It is important to bear in mind that reddening would add another important parameter affecting the galaxy spectra, in particular the shape of the continuum and the relative intensities of the emission lines, although not the equivalent width of the absorption features.

3 PRINCIPAL COMPONENT ANALYSIS

Suppose we have a sample of N galaxy spectra, all covering the same rest-frame wavelength range. Each spectrum is described by an M-dimensional vector X containing the galaxy flux at M uniformly sampled wavelengths. Let S be the M-dimensional space spanned by the 'spectral' vectors X. A given spectrum, then, is a point in S-space, and the spectra in the sample form a cloud of points in S. The position of a galaxy spectrum point in this space depends on parameters such as age, star formation history and metallicity. However it is impossible to visualise directly how the data are distributed in high dimensional spaces. An alternative is to employ some technique for dimension reduction by projecting the data in, say, two dimensions.

Here we analyse the data with a standard technique, Principal Component Analysis (PCA). commonly used in Astronomy (e.g, Murtagh & Heck (1987) and references therein). The PCA method is also known in the literature as Karhunen-Loéve or Hotelling transform.

PCA is an orthogonal transformation that allows the building of more compact linear combinations of data that are optimal with respect to the mean square error criterion. The new orthogonal basis is composed of vectors called Principal Components (PCs). The first Principal Component is taken to be along the direction in the S space with the maximum variance of data points X. More generally, the k-th component is taken along the maximum variance direction in the subspace perpendicular to the subspace spanned by the first $(k-1)$ Principal Components.

The formulation of standard PCA is as follows (see e.g. Murtagh & Heck 1987). Consider a set of N objects ($i = 1, N$), each with M parameters ($j = 1, M$). If r_{ij} are the original measurements, we construct normalised properties as follows:

$$X_{ij} = r_{ij} - \overline{r}_j, \quad (1)$$

* In the synthetic spectra, the [OIII] λ4959Å–λ5007Å doublet is represented by the λ5007Å line only. Since the intensity of the λ4959Å line is always $\frac{1}{3}$ that of the λ5007Å line, there is no loss of information.

where

$$\overline{r}_j = \frac{1}{N}\sum_{i=1}^{N} r_{ij} \tag{2}$$

is the mean. We then construct a covariance matrix

$$C_{jk} = \frac{1}{N}\sum_{i=1}^{N} X_{ij}X_{jk} \quad 1 \le j \le M \quad 1 \le k \le M. \tag{3}$$

It can be shown that the axis along which the variance is maximal is the eigenvector $\boldsymbol{e_1}$ of the matrix equation

$$\mathbf{C}\boldsymbol{e_1} = \lambda_1 \boldsymbol{e_1}, \tag{4}$$

where λ_1 is the largest eigenvalue, which is in fact the variance along the new axis. The other principal axes and eigenvectors obey similar equations. It is convenient to sort them in decreasing order, and to quantify the fractional variance by $\lambda_\alpha / \sum_\alpha \lambda_\alpha$. It is also convenient to renormalize each component by $\sqrt{\lambda}_\alpha$, to give unit variance along the new axis. The sign $(+/-)$ of the eigen-vectors is arbitrary. We note that the weakness of PCA is that it assumes linearity and also depends on the way the variables are scaled. In the analysis which follows, the spectra are all normalised to have the same total flux over the wavelength range considered. This is a simple and convenient choice which preserves the shape of the spectrum.

The matrix of all the eigenvectors forms a new set of orthogonal axes which are ideally suited to a description of the data set. If the main variance of the data set lies in a small dimensional space, then one can get a good visualisation of it by plotting the data projected on the first few eigenvectors (PCs), the projection of a vector v on the eigenvector $\boldsymbol{e_i}$ being $\boldsymbol{v} \cdot \boldsymbol{e_i}$. The fractional variance of the first PCs tells us to what extent the data lie in a given low dimensional space. In what follows, we will apply this technique to different model galaxy samples. To avoid confusion we denote eigenvectors by PC1,PC2 etc. and projections on the new axes by pc1, pc2 etc.

4 SINGLE BURST GALAXIES

We used PEGASE to simulate the spectra of galaxies formed in a single instantaneous burst that takes place at $t = 0$ in the age range 0–18.5 Gyr. Figure 1 shows some of the model spectra at different ages. For our first study, we simulated 1850 spectra between 10 Myr and 18.5 Gyr in equal time intervals of 10 Myr, and performed PCA on this sample. However, we found that by 10 Myr emission lines already decay to a negligible value compared with the continuum. To see the change in emission lines in very early ages, we also performed PCA on a sample of 15 spectra with ages 0–15 Myr and time step of 1 Myr.

Figure 2 shows the mean of the 1850 spectra along with the first three eigenvectors. The first PC (PC1) accounts for 98.5% of the variation in the spectra. It correlates blue continuum with Balmer absorption lines. What seems like some emission in the Mgb and NaD lines represents compensation for the absorption in this lines in the average spectrum. Also note that the blue spectrum is correlated with the negative of broad absorption features in the red end (6000–7000Å) which appear in the average spectrum. We identify these as

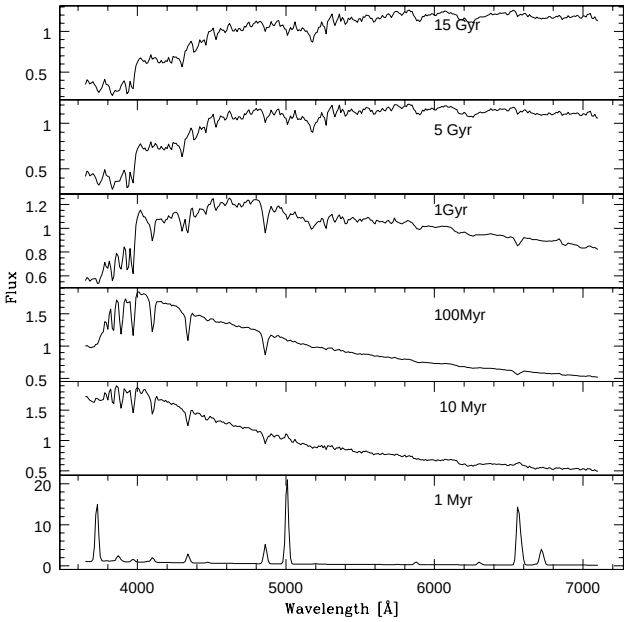

Figure 1. Model spectra for different galaxy ages computed with the PEGASE code for stellar populations formed in an instantaneous burst. The spectra are normalised to the same constant total flux over the wavelength range of interest.

typical molecular absorption lines of an M-star spectrum. The physical significance of this is that as a galaxy ages, later type stars contribute more relative flux to the integrated spectrum and it becomes redder, so the M-star spectral features should be anti-correlated with blue colour. The second principal component, PC2, accounts for only 0.9% of the variation, therefore any features present in it (e.g., the strong Ca K absorption) represent only fine tuning to the main variation which PC1 represent. PC3 accounts for only 0.5% of the variation. It correlates the Balmer absorption lines with absorption below 4000Å, i.e, the Balmer break.

To demonstrate the use of the PCA to determine the age of a galaxy from its spectrum we plot in Figure 3 the projection on the first PC (pc1) versus age. This is mainly a monotonically decreasing curve, clearly showing the reddening of the galaxy spectrum with age. Note that the slope becomes much shallower at later ages, reflecting the slower change in spectral shape at old ages since the lifetime of the main stellar contributors becomes larger. This makes accurate age determinations more difficult for old galaxies. Some small non-monotonic irregularities in the curve are probably due to abrupt transitions of stars to different evolutionary stages. They may be real, but they may also occur if the model does not contain enough evolutionary tracks in a certain range. In any case, we shall see that these irregularities will be smoothed out when considering longer and more realistic (continuous) star formation histories instead of the instantaneous bursts considered here.

In figure 4 we plot the projection on the PC1–PC2 plane. The turning point in the graph correspond to an age around 400 Myr, and the PC2 maximum corresponds to 770 Myr. Since one of the the dominant features of PC2 is the Ca K absorption line, this suggests a maximum for

K absorption around that time. To check this hypotheses, we plot in figure 5 the equivalent width of the K absorption line versus age. There is a sharp rise in absorption at early ages, and a turning at 2 Gyrs to a rather flat curve. Overall there is a good correspondence with the PC2 behaviour, but the maximum occurs at later age. This happens because PC2 contains other features as well, in particular a strong 'Balmer decrement' below $\simeq$ 4000Å which makes the projection negative for very blue young galaxies, and a slightly blue slope above 4000Å that makes the projection become negative for old galaxies. Note that the Ca H line appears to behave differently from the Ca K line. This is due to the close proximity of the Balmer Hϵ line, whose strength often anti-correlates with that of the Ca H line.

The Ca K line and other metallic absorptions appear in a different PC than the Balmer lines because the metal lines develop later than the Balmer series, as an examination of figure 1 reveals. This is easily understood in terms of the spectral properties of the dominant stellar types at each age: young A spectral type stars dominate when the galaxy is $\simeq$ 1 Gyr old, while stars with strong metallic lines have lower masses, thus dominating at later ages. The hydrogen absorption lines are correlated with the blue spectrum of PC1, while the metallic absorptions are correlated with the redder spectrum of PC2 and with the 4000Å break. These are typical features of a spectrum older than 1 Gyr (figure 1), where the metallic absorptions (e.g., Ca K) are strong. This simple exercise demonstrates how PCA, which does not 'know' anything about stellar evolution or stellar spectra is able to identify the main contributors to a galaxy spectrum as it evolves.

We now turn to the analysis of very young populations with strong emission lines, aged 0–15 Myr. Figure 6 shows the mean spectrum and the first PCs of a sample of galaxies with ages 0–14 Myr and a sampling interval of 1 Myr. First note that the average spectrum is indeed that of a very young galaxy: blue continuum with emission lines. The first PC contains mainly emission lines, with especially strong Hα and Oxygen lines. The energy source of this emission is the UV photons (below the Lyman break at 912Å) of very young blue stars absorbed by the inter-stellar gas and then re-emitted by recombination and radiative/collisional de-excitation. The first PC accounts for 99.5% of the variation in this sample. The second PC now is basically a blue continuum, and is responsible for 0.7% of the variation. The third PC represents only 0.05% of variation. It shows absorption lines correlated with absorption below the Balmer break at 4000Å, but also with persisting emission in Hα and Oxygen lines —these being the strongest and the last ones to decay.

Figure 7 shows the change of the PC1 and PC2 components with time. The PC1 projection shows that emission lines dominate only at very young ages after the initial star burst. Emission and/or partial filling of absorption lines continue up to 6 Myr, becoming much weaker at later ages. The PC2 projection shows that the continuum is maximally blue about 3–5 Myr after the burst, and then becomes less blue. We interpret the sharp drop at 8 Million year as signalling the beginning of the death of the most massive, bluest and most luminous stars.

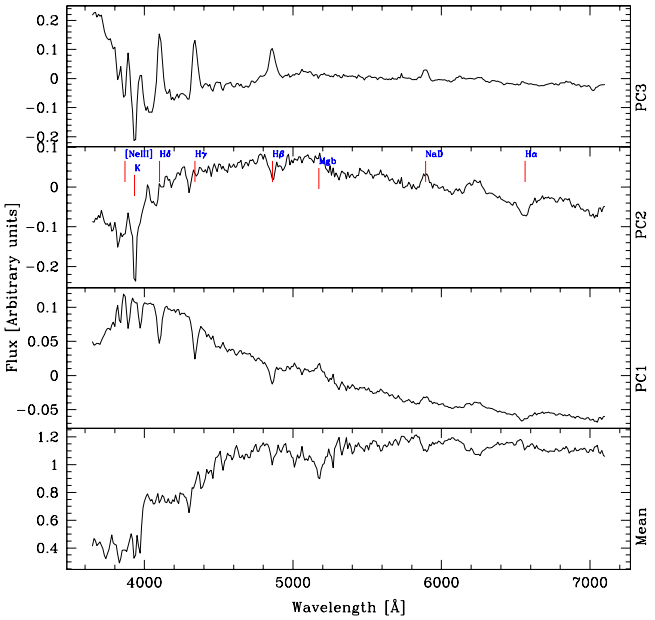

Figure 2. Single burst: the mean of the 1850 synthetic spectra of galaxies formed in a single instantaneous burst that takes place at $t = 0$ in the age range 0.01–18.5 Gyr in equal time intervals of 10 Myr (bottom). The first three PCs are plotted above it. The wavelength of some atomic line features are marked. Note that these may represent either emission or absorption, depending on the sign of the weight factor multiplying each PC. The PC1,PC2 and PC3 correspond to a variance in the spectra of 98.5%, 0.9% and 0.5%.

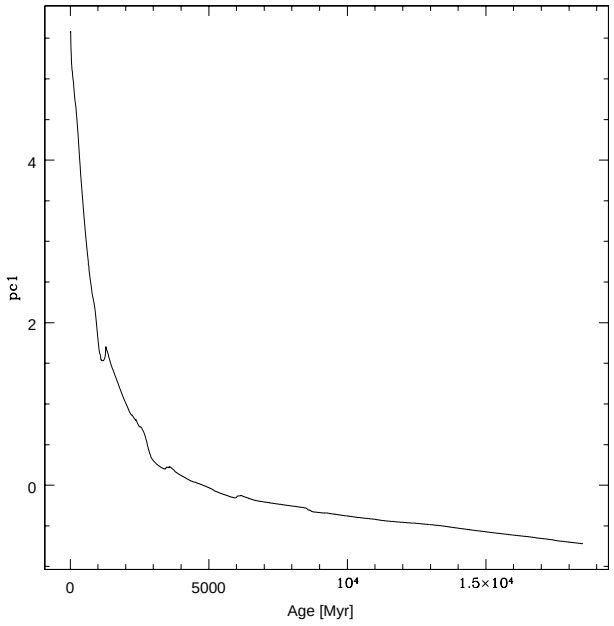

Figure 3. Single burst: the projection of the spectra on the first PC of figure 2 versus age.

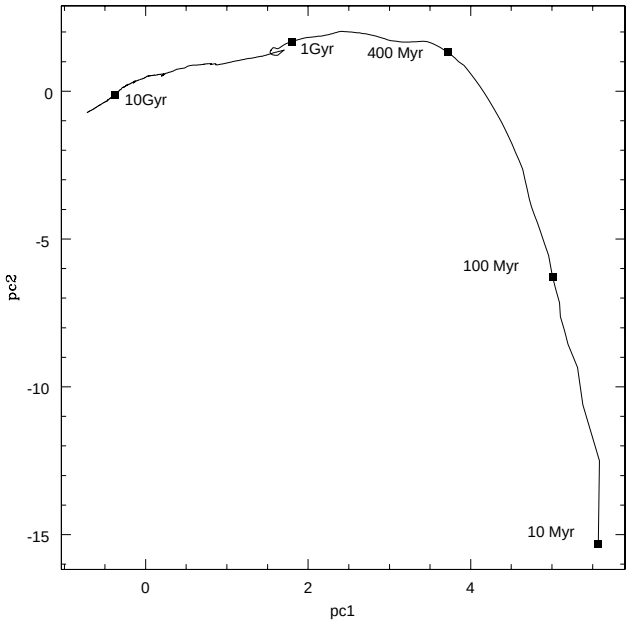

Figure 4. Single burst: the projection of the spectra on the first and second PCs of figure 2. The ages are marked.

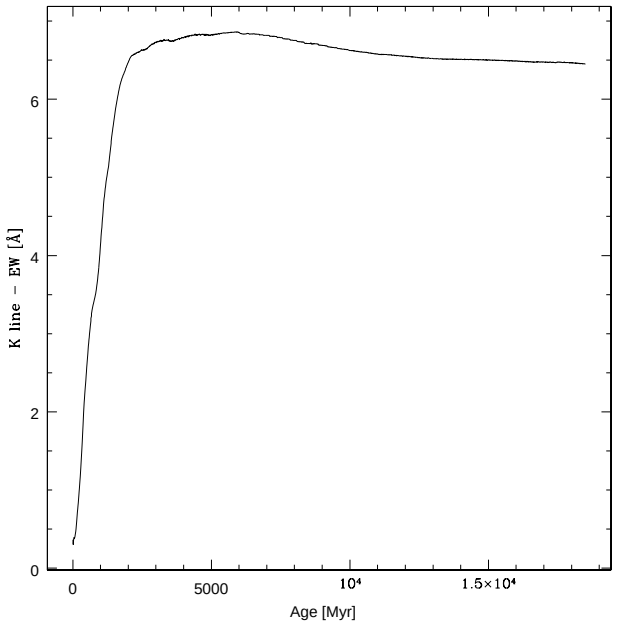

Figure 5. Single burst: The equivalent width of the Ca K line (λ3933Å) versus age.

5 GALAXIES WITH A CONTINUOUS STAR FORMATION HISTORY

In reality, the stellar populations of most galaxies are not formed in a single instantaneous burst. Commonly continuous star-formation rate at time t is modelled by

$$SFR = (1/\tau)\exp(-t/\tau)\ , \qquad (5)$$

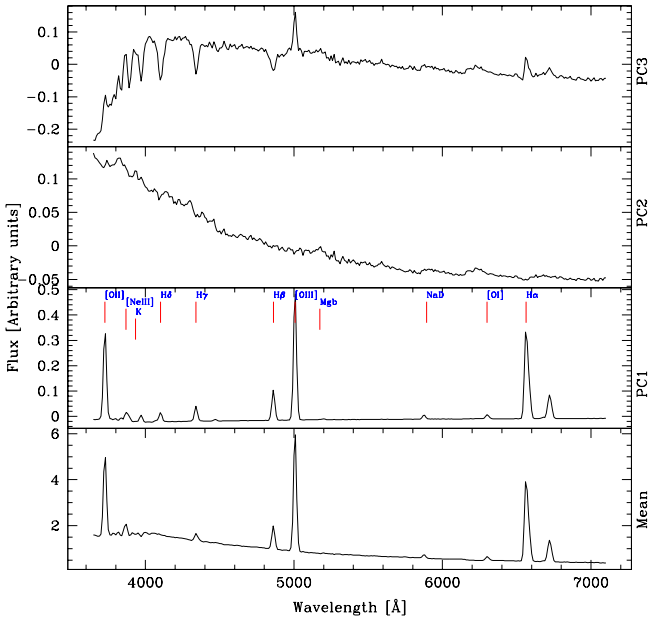

Figure 6. Early single burst: the mean of the synthetic spectra of galaxies formed in a single instantaneous burst that takes place at $t = 0$ in the age range 0–14 Myr in equal time intervals of 1 Myr (bottom). The first three PCs are plotted above it. PC1, PC2 and PC3 correspond to a variance in the spectra of 99.5%, 0.7% and 0.05%.

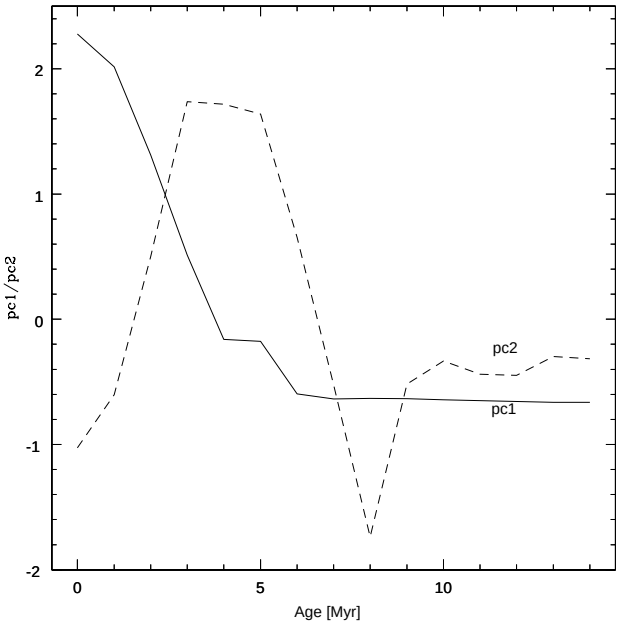

Figure 7. Early single burst: the projection of the 0–14 Myr spectra on the first and second PCs of figure 6 versus age.

where τ is the e-folding time. Spiral galaxies seem to be best fitted by exponentially decreasing star formation rates (SFRs) with e-folding times of the order of several Gyrs, while ellipticals are best fitted with models with much shorter star-formation time scales ($\tau \simeq 1 Gyr$; see, e.g., Tinsley 1980; Bruzual 1983)

The difficulty of ascribing a certain age and star formation history to a galaxy is that young age and a significant current star formation seem to give the same effect on the spectrum: blue light from young stars with strong Balmer and other emission lines. The reason for this is that the blue young stars are the most luminous objects in the galaxy and dominate its spectrum. One would like to find a way to separate these two important parameters from the galaxy spectra.

With this aim, we analyse a sample of galaxy spectra of ages 0.1–18.5 Gyr with a time step of 100 Myr and exponential SFR with e-folding time τ in the range 0–7 Gyrs. We have chosen the values $\tau = 0, 0.1, 0.5, 1, 2, 3, 5, 7$ Gyr ($\tau = 0$ means single instantaneous burst, as in our previous analysis). Figure 8 shows the mean spectrum and the first PCs of this sample. The contributions of the PCs to the variance are: PC1 97.08%, PC2 2.75%, PC3 0.13%, and so again the sample is fitted well by a line along PC1. Note the anti-correlation between emission and absorption lines in it. This is in agreement with our previous discussion of young single star-burst populations: the competition between the physical processes of absorption in the stellar atmospheres and gas emission produce stronger emission in the Oxygen lines and Hα and absorption in higher H lines. Still, at younger ages we expect more emission, and as we shall see, this is shown by the *negative* values of PC2 (which has correlated *absorption* lines). The prominent feature in PC3 is again absorption in Ca K line. It is very interesting and encouraging that the first two PCs, derived here from synthetic spectra, are very similar to the ones obtained from a sample of observed galaxies —see the analysis of Folkes et al. (1996) using Kennicutt's (1992) data and the analysis of the 2dF data (Folkes 1998).

In figure 9 we plot the PC1 projection versus age for all the star formation histories. We see that, at a given age, galaxies with SFR histories of larger e-folding times, (i.e., more star formation at later ages), have bluer spectra and more emission lines. This is to be expected since when the star formation time scales become longer (larger e-folding times), the ratio of the current star formation rate to to average past SFR becomes larger (i.e., newly-formed stars contribute more, in relative terms, than stars formed in the past —recall that we normalise the spectrum by total flux). Therefore, the ratio of the current SFR over the average past SFR (or total stellar mass), sometimes known as the 'Scalo Parameter', is very important in determining the spectrum of a galaxy. A simple calculation shows that this parameter is monotonically increasing with τ at any age for exponentially-decaying star-formation histories.

The resulting ambiguity in age/SFR history is particularly severe for redder galaxies, i.e. older ages. To resolve it we proceed to look at the next PCs. Figure 10 is a projection on the PC1–PC2 plane. First note the general trend: bluer (i.e. younger) galaxies with large PC1 have enhanced emission lines (negative PC2). With a starting age of 100 Myr, the single burst spectra (top curve) already lack emis-

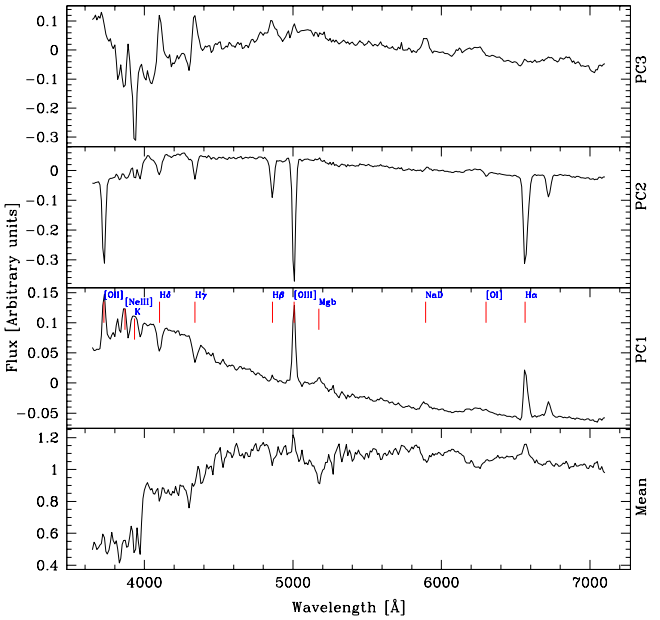

Figure 8. Continuous star formation: the mean of the synthetic spectra of galaxy models with continuous exponentially decaying star formation histories aged 0.01–18.5 Gyr (bottom —see text for details). The first three PCs are plotted above it. PC1, PC2 and PC3 correspond to a variance in the spectra of 97.08%, 2.75% and 0.13%.

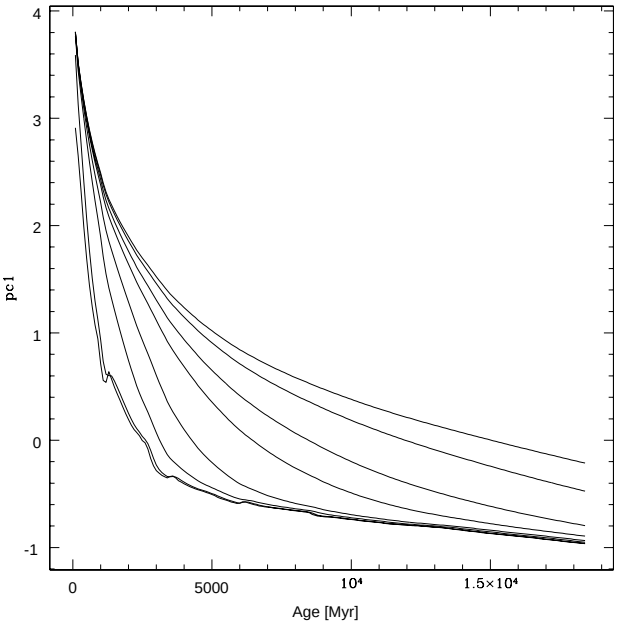

Figure 9. Continuous star formation: the projection of model galaxy spectra with continuous star formation histories on the first PC of figure 8 versus age. The lowest line corresponds to $\tau = 0$ Gyr, followed by $\tau = 0.1, 0.5, 1, 2, 3, 5, 7$ Gyr in ascending order.

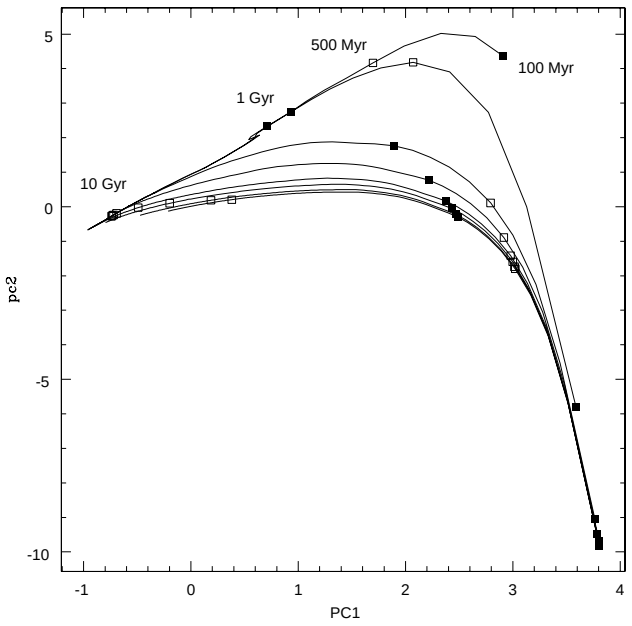

Figure 10. Continuous star formation: the projection of galaxy spectra with continuous star formation histories on the first and second PCs of figure 8. The top line corresponds to $\tau = 0$, followed by $\tau = 0.1, 0.5, 1, 2, 3, 5, 7$ Gyr in descending order. The alternating open and closed boxes indicate ages of 0.1, 0.5, 1 and 10 Gyr.

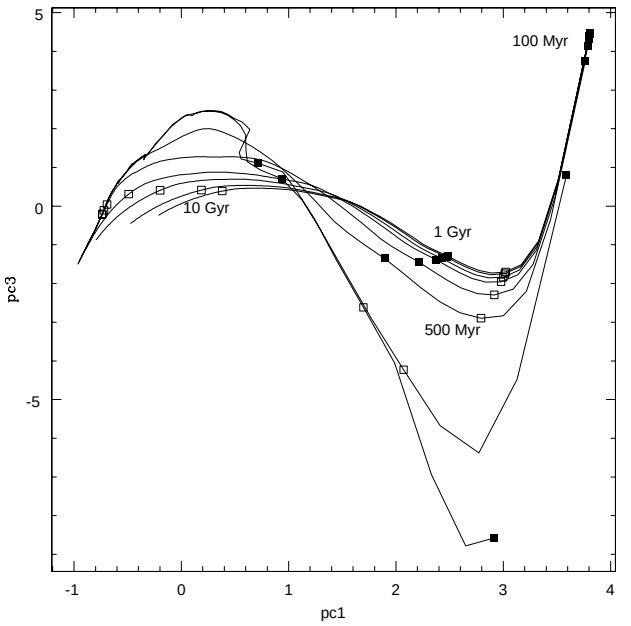

Figure 11. Continuous star formation: the projection of galaxy spectra with continuous star formation histories on the first and third PCs of figure 8. At the left of the figure, the top line corresponds to $\tau = 0$, followed by $\tau = 0.1, 0.5, 1, 2, 3, 5, 7$ Gyr in descending order. The alternating open and closed boxes indicate ages of 0.1, 0.5, 1 and 10 Gyr.

sion lines, but show enhanced absorption lines instead. This is in accordance with our result in the previous section. The SFR histories with τ between 0 and 2 Gyrs are well separated around PC1 = 2.0, indicating more emission strength for blue galaxies with higher τ. However looking back at Figure 9, this applies to galaxies of $age < 2$ Gyr. For older and therefore redder galaxies with smaller PC1 component, the curves in the PC1–PC2 plane tend to converge, and do not provide a good separation. Also for the range of τ between 2 and 7 Gyrs, all curves are very much the same over the whole range. We should therefore turn to the third PC.

Figure 11 shows a projection on the PC1–PC3 plane. Although harder to interpret, it does seem to give us some separation in the parameter range of interest. A word of caution: the variance in PC3 (0.13%) is very small, and noise in real integrated spectra may cause a large dispersion here. The extent of noise degradation is discussed in section 7.

6 THE EFFECT OF METALLICITY

In this section address the issue of different metalicities in the stellar populations of the galaxies and their impact on the spectra. Again, we want to to separate the effects of metallicity and age on the integrated galaxy spectra. Specifically, we apply it to old and simple stellar populations, which could represent those of elliptical galaxies.

Worthey (1994) investigated this problem by computing colours and individual line indices in elliptical galaxy models, and studying the variation of the different observables individually when changing age and metallicity. Here we apply the PCA technique to the problem, studying the global properties of the spectra simultaneously, instead of one feature at a time. As described in section 2, we use the Multi-metallicity Isochrone Synthesis Spectral Evolutionary Code of Bruzual & Charlot (1996), based on theoretical stellar spectra. The six different metalicities available have the following mass fraction Z of elements heavier than Helium: $Z = 0.004, 0.040, 0.080, 0.0200, 0.0500$ and 0.1000. In this scale, the solar metallicity is about $Z = 0.02$. Using the BC models, we sampled ages between 250 and 18500 Myr with a step of 250 Myr, and performed PCA on a single burst model sample including all six metalicities. Emission lines become negligible in this age range for single burst models.

Figure 12 shows the mean spectrum and the first PCs of this sample. The contributions of the PCs to the variance are: PC1 96.41%, PC2 2.03%, PC3 0.34%. The average spectrum and the first PC are very similar to those shown in figure 2 for a single solar metallicity population, although now there is a larger variance associated to the metallic lines, as expected for a sample of galaxies which contain a mixture of metalicities. In PC1 some of the metallic lines appear as 'emission' features (e.g., the NaD, Mgb, and Fe lines). These are in fact absorption lines, but anti-correlated with Balmer absorption lines and blue colours. This in accordance with the results of Worthey (1994). PC2 is very different from the one shown in figure 2. The variance in it is bigger than in the case of single solar metallicity, reflecting the larger variance in the sample due to metallicity effects. It contains metallic absorption features: NaD, Mgb, Fe5015, Fe5782. The most

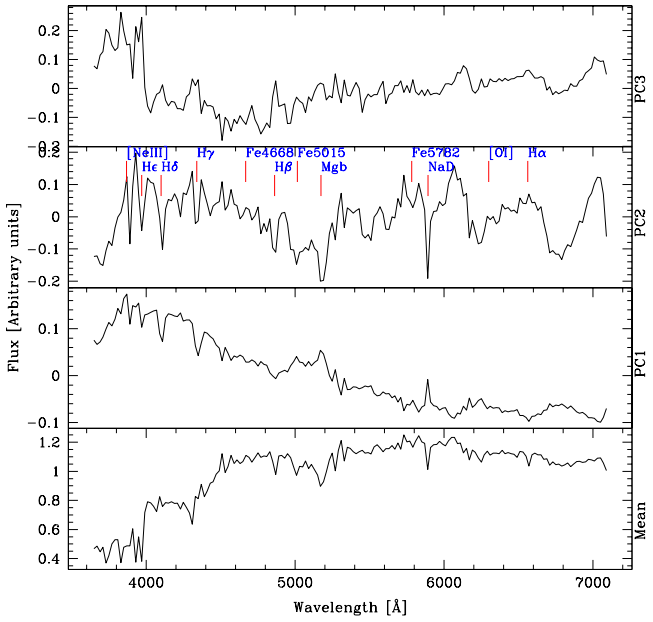

Figure 12. Metaliciy effects: the mean of the synthetic spectra of stellar populations with different metalicities aged 100–1850 Myr (bottom), and the first three PCs plotted above it. PC1, PC2 and PC3 correspond to a variance in the spectra of 96.41%, 2.03% and 0.34%

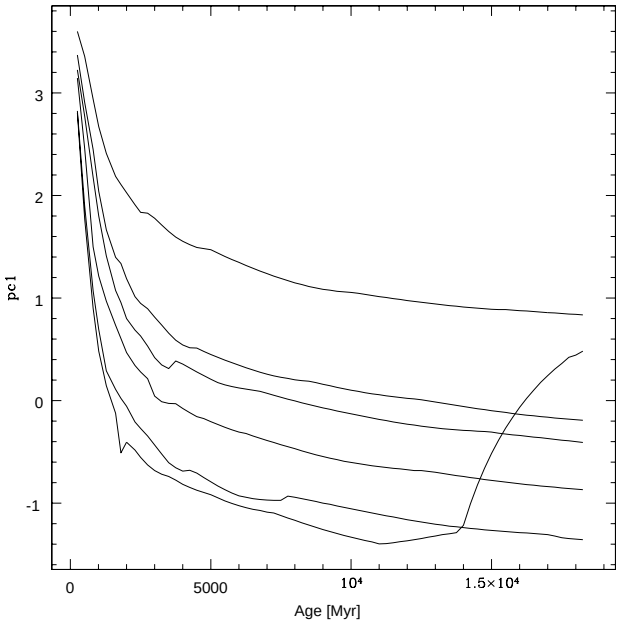

Figure 13. Metallicity effects: the projection of spectra of different metallicity on the first PC of figure 12 versus age. The bottom line corresponds to $Z = 0.1$, followed by $Z = 0.05, 0.02, 0.008, 0.004$ and 0.0004

dominant are NaD† and Mgb absorption lines. PC2 also contains Balmer absorption lines, this time positively correlated with the metallic lines. We explain this in the discussion of figure 14 below.

In figure 13 we plot the PC1 projection versus age for all the metalicities. Since PC1 as a blue continuum slope, we see a clear uniform tendency for galaxies to become redder with increasing metallicity. The exception are the models with the highest metallicity, which become much bluer after 14Gyr. Bruzual & Charlot (1996) explanation for that behaviour is the appearance of AGB-manqué stars at $Z = 0.1$, which due to a very efficient mass loss skip the AGB phase and instead go through a long lived hot HB phase. That could explain the UV-upturn seen in the spectra of massive (i.e., high metallicity) ellipticals. However, these authors warn that this particular result should be taken with caution, as the evolutionary tracks of high metallicity stars are quite uncertain. At any rate, $Z = 0.1$ is 5 times the solar metallicity and observationally very uncommon.

In figure 14 we plot the projection of the sample on the PC1–PC2 plane. In general, a population with higher metallicity occupies a locus with higher PC2 for a given PC1 (or colour). However, this is not true for a given age: for 10 Gyr, higher metallicity gives higher PC2, but for 1 Gyr it gives lower PC2. The explanation for this as follows: in general, for a given age, the strength of the Balmer absorption lines decreases with metallicity (as already seen by Worthey 1994). At 1 Gyr the Balmer lines are strong and dominate the projection on PC2. At 10 Gyr, the Balmer lines are weak and the metallic absorption lines dominate the projection on PC2. The correlation between metallic and Balmer lines in PC2 indicates that this is indeed the case, in a statistical sense, for a given PC1 (or colour).

We conclude that the fact that the first PC already accounts for 96.41% of the variation shows that there is indeed an age-metallicity degeneracy, but the use of the second PC allows us to separate them in principle. It may be argued that, from its definition, the PCA method is the optimal way to achieve such a separation (at least using linear methods). PCA is also simple, since there is no need to calculate a multitude of photometric colours and spectral indices: all the spectral features are taken into account *simultaneously, in an optimal way.*

7 THE EFFECT OF NOISE

When it comes to the analysing of real observed spectra, one of the major concerns is the signal to noise (S/N) ratio. In previous sections we have shown that information contained in the second or third PCs may enable us to separate the effects on the spectra of different star formation histories or metalicities from age, thus determining all these parameters simultaneously. However, as we have shown, the relative variance contained in the second and third PCs is generally very small, of order of one percent. Therefore, in order to suggest PCA as a practical method for the above task, we need to pay careful attention to the effect of noise. Noise affects both the eigenvectors and the projection of objects into the PCA space.

Let N_p be the total number of photon counts in a given

† Nad is a resonant line, and could be affected by interstellar absorption, which the models do not include.

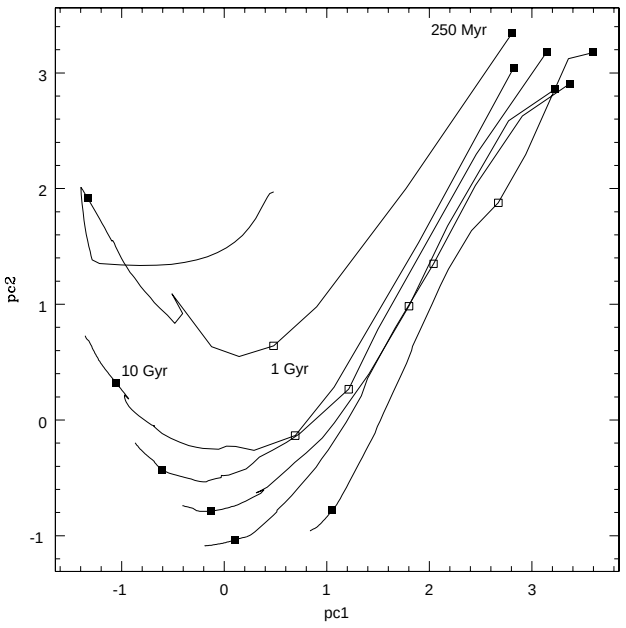

Figure 14. Metallicity effects: The projection of spectra of different metallicity on the PC1–PC2 plane. The top line corresponds to $Z = 0.1$ followed by $Z = 0.05, 0.02, 0.008, 0.004, 0.0004$ (the lines do not cross over in the middle). The alternating open and closed boxes indicate ages of $0.25, 1$ and $10\,$Gyr.

spectral bin, and let us assume that photon number counts obeys Poisson statistics. Usually N_p will get contributions both from the galaxy flux and from the sky spectrum, however for the sake of our analysis we ignore the sky contribution (See Folkes et al. 1996 for simulations including sky contribution). Define the signal S to be the expectation value of the number of counts:

$$S = \langle N_p \rangle \ . \tag{6}$$

Then the signal to noise ratio in this bin is just:

$$S/N = \sqrt{S} \ . \tag{7}$$

The noise variance is added to the diagonal of the covariance matrix (eq. 3), as the noise in different bins is supposed to be uncorrelated. For a realistic galaxy spectrum the noise in each bin is different (as it depends on the galaxy flux at each bin). Hence the addition of noise may rotate the eigenvectors to different directions compared with the noise-free case (if the noise is constant per bin then the direction of the eigenvectors is not affected, only the eigenvalues are changed). However, one expects, and our experiments confirm, that the first eigenvectors corresponding to large intrinsic variance in the clean data will be little affected by noise. Also note that the noise in the eigen-spectra will be reduced with the size of the sample spectra, because of the averaging of the covariance matrix over all the spectra in the sample.

Another effect of the noise in spectra will be that, even if eigenvectors do not chance direction, noise in a given spectrum will change its projection into the PCA space. This will introduce scatter in projection plots, such as pc1-pc2 plots presented in this work. It will increase the PCA eigenvalue corresponding to any PC. We wish to derive here a simple mathematical expression for this effect, under the following assumptions. Let us consider a simplified case in which the clean spectrum is a flat line. Then the S/N is constant over the whole wavelength (even if the clean spectrum is not flat, then, to a first approximation, we can take the S/N to be a constant, equal to the average signal to noise over the observed wavelength range). Secondly, let us examine a sample of galaxies with the same apparent magnitude, so that the S/N is the same for all galaxies in the sample. Also let us assume that the eigenvectors of interest are largely unaffected by the noise (but see below for a more careful examination of this assumption).

Then we can calculate the noise in the projection coefficients and the resulting change in eigenvalues as follows. As usual, the spectra are first normalized to have a constant total flux. For convenience we choose a normalization such that the average normalized counts per bin is 1. I.e, we are dividing N_p by S. Then the variance of N_p in this normalization, which we denote by V, is:

$$V = Var(N_p/S) = Var(N_p)/S^2 = 1/S = 1/(S/N)^2. \tag{8}$$

Therefore V is the (renormalized) variance of noise in each bin. Under our assumptions this is the same for all bins, i.e, the noise is isotropic. Hence, after the orthogonal transformation to the PCA basis, the contribution of noise to the variance in each PC direction will be the same for all PCs, and equal to V. In other words, when calculating the projection coefficients of a given galaxy spectra on a given PC, each coefficient will include noise with a variance of V.

If in the absence of noise the eigenvalue of a given eigenvector i of the covariance matrix is λ_i, then in the presence of noise this eigenvalue becomes $\lambda_i + V$. Taking a square root to move from variances to standard deviations, we conclude that the ratio

$$Q_i \equiv \sqrt{\frac{V}{\lambda_i}} = \frac{1}{(S/N) \cdot \sqrt{\lambda_i}} \tag{9}$$

gives us a measure of the relative spread in PCA projection coefficients due to noise, as compared with the internal variance in the data due to galaxies having different spectra. The requirement for a projection on a given PC to be relatively noise free is therefore $Q_i \gg 1$, or:

$$S/N \gg 1/\sqrt{\lambda_i} \ . \tag{10}$$

This last expression, although a crude approximation, is useful for planning observations to discriminate between age/sfr/metallicity using the PC projections presented above.

For example, in the study of single burst galaxies we found that $\lambda_1 = 3.96$, $\lambda_2 = 0.035$ and $\lambda_3 = 0.020$. Therefore, for PC1, PC2 and PC3 projections to be meaningful the signal-to-noise S/N must be larger than 0.5, 5.3 and 7.1 respectively (per $10\mathring{A}$ spectral bin which is the resolution considered here). The PC1 projection is therefore negligibly affected by noise while PC2 and PC3 require very high S/N.

In the analysis of continuous star formation histories there is a larger variance in PC2, corresponding to (i.e., requiring) a minimum $S/N = 2$. For PC3, a $S/N = 10$ is required. In the analysis of galaxies with different metalicities we get $S/N = 3.6$ for PC2 and $S/N = 5.3$ for PC3. For example, to really differentiate between two consecutive metallicity curves of figure 14, a significantly smaller scatter

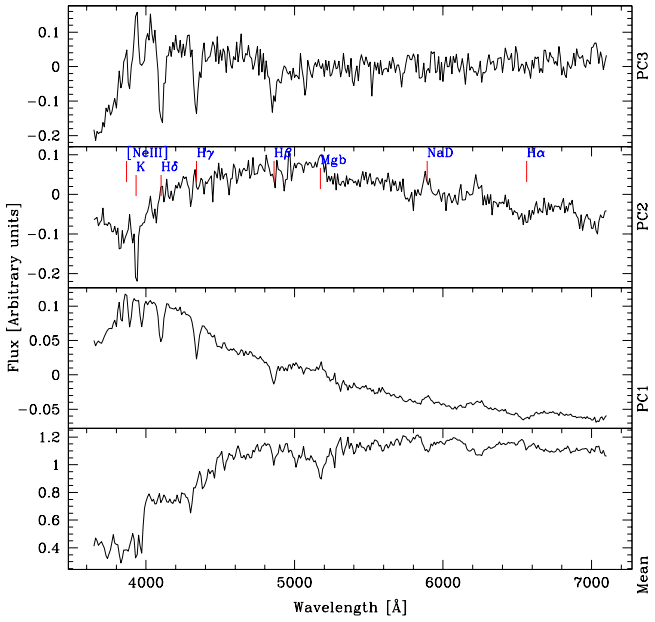

Figure 15. The effect of noise, with a $S/N = 10$, on the PCs of single burst stellar population spectra, to be compared with figure 2. PC1, PC2 and PC3 correspond to a variance in the spectra of 52.2%, 0.6% and 0.4%

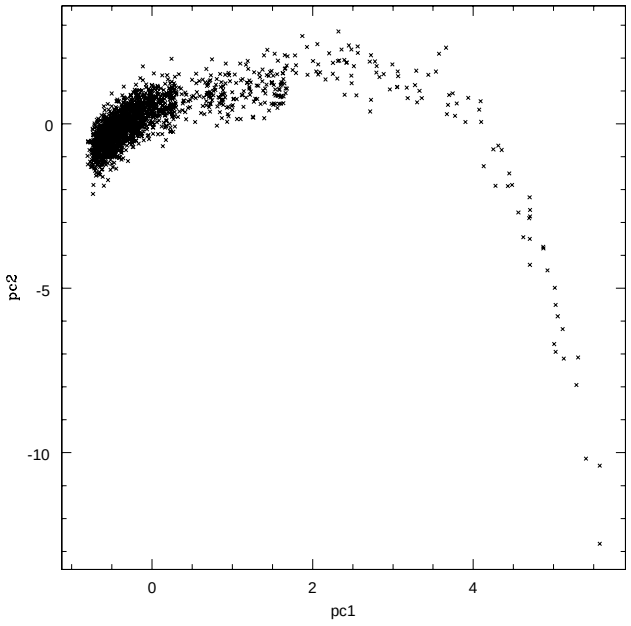

Figure 17. Effect of noise: The projection of the noisy spectra on the first and second PCs of figure 15, to be compared with figure 4.

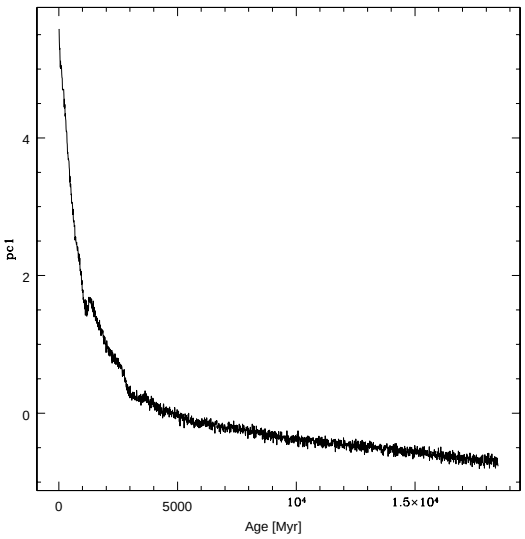

Figure 16. Effect of noise: The projection of the noisy spectra on the first PC of figure 15 versus age, to be compared with figure 3.

then the whole pc2 variance is required, and the required S/N should be scaled up accordingly.

We concluded in previous sections that to separate age from SFR history, one will need PC3, while to separate age from metallicity PC2 is enough. Therefore, the above numbers indicate that a $S/N > 10$ per wavelength element (at $\simeq 10$Å resolution) may already enable some metallicity discrimination (between the highest and lowest metallicity values), but higher quality spectra are required to determine the star formation history separately from the age.

To illustrate in a more realistic way the effect of noise discussed above, we have performed a numerical simulation. We returned to the analysis presented in section 4 of single burst population with ages 0–18.5 Gyr, but this time with (a Poisson) noise added to the synthetic spectra. For each galaxy, we assumed a magnitude such that the average photon counts per bin is 100. This corresponds to a $S/N = 10$ in our simplified analysis above. However, in the simulation we did include a S/N which properly changes from bin to bin according to flux. Figure 15 shows the resulting PCs, to be compared with figure 2. The noise little affects the average spectrum and the first PC, while the third PC is more significantly degraded. Also, PC1, which previously accounted for 98.5% of the variance of the sample, now accounts for only 52.2% (PC2 0.6%, PC3 0.4%), and much of the variance, due to noise, is more or less evenly distributed between PC's higher than the third one. Figure 16 shows the projection of the noisy spectra on the first PC, to be compared with figure 3. As expected, the PC1 projection is affected by the noise only slightly. Figure 17 shows the projection of the noisy spectra on the PC1–PC2 plane, to be compared with figure 4. Significant noise enters the PC2 projection, but it is still less than the total variance in PC2, as could be expected from the simple calculations above.

8 DISCUSSION

In this study we applied PCA to synthetic spectra with different ages, star formation histories and metalicities. The PCA provides a more objective and informative alternative to diagnostics by individual spectral lines, as in the PCs rep-

resent all the spectral features *simultaneously*. In particular it is encouraging that our first two synthetic PCs agree with a similar analysis on observed spectra obtained by Kennicutt (e.g. Sodre & Cuevas 1997; Folkes et al. 1996) and the new 2dF redshift survey (Folkes 1998).

Our first experiments with single burst populations show, as expected, the significant effect of the sampling on the resulting PCs. I.e, when one samples young galaxies the first PCs reflect the main variance in that young age which is different from that for an older population. In examining data from big spectral surveys we do not know a priori how many galaxies are of each age. Therefore it seems best to derive the PCs (eigenvectors) from the observational data, and then project on them both the observational data and the synthetic model spectra in order to find the best fit parameters (age, SFR, metallicity) for the observed galaxies. The disadvantage of deriving the PCs from the observational data is the effect of noise on the eigenvectors themselves. However, any systematic effect due to noise anisotropy will be small for the first eigenvectors, and the random effect will be reduced with the inverse square root of the number of spectra, which is encouraging for the coming big spectral surveys (2dF, Sloan). Alternatively, one can project the observational data on the theoretical PCs derived from some pre-chosen synthetic sample of ages (and other parameters). The statistical composition the synthetic spectra may be chosen on some theoretical grounds, or experimentally, from the first procedure just outlined. We shall discuss elsewhere various approaches to this 'inverse problem'.

When there are only two parameters such as age and SFR or age and metallicity, our experiments suggest the possibility to determine them separately from the first two or three PCs, given a good enough S/N ($S/N \gg 10$ for metallicity and better for SFR discrimination). In practice all three are involved, including others, such as chemical evolution, extinction by dust, etc. However assuming the first three are responsible for the major variance in the spectra, our analysis suggests that a parameter fit using the PCA method may be successful for high quality spectra. This analysis highlights the need for a large sample of high signal-to-noise of galaxy spectra.

ACKNOWLEDGEMENTS

We thank S. Folkes and K. Glazebrook for helpful discussions and G. Bruzual, S. Charlot, M. Fioc & B. Rocca-Volmerange for providing easy access to their model calculations. S. Ronen is grateful for a scholarship from Trinity College, Cambridge, and A. Aragón-Salamanca acknowledges generous financial support by the Royal Society.

REFERENCES

Bailer-Jones C.A.L., Irwin M., Gilmore G., von Hippel T., 1997, MNRAS, 292, 157

Bromley, B.C., Press, W.H., Lin, H., Kirshner, R.P, 1998, ApJ, submitted

Bruzual, G., 1983, ApJ, 273, 105

Bruzual G., Charlot S., 1996, Galaxy Isochrone Synthesis Spectral Evolution Library, Multi Metallicity Version (GISSEL96)

Bruzual G., Charlot S., 1993, ApJ, 405, 538

Colless M.M., 1998, 'Looking Deep in the Southern Sky', eds Morganti R., Couch W.J.,ESO/Australia workshop, Springer, in press

Connolly A.J., Szalay A.S., Bershady M.A., Kinney A.L., Calzetti D., 1995, AJ, 110, 1071

Fioc, M., Rocca-Volmerange, B., 1997, A&A, 326, 950F

Folkes S.R., Lahav O., Maddox S.J., 1996, MNRAS, 283, 651

Folkes, S.R., 1998, PhD thesis, Cambridge University

Francis, P.J., Hewett, P.C., Foltz. G.B., Chaffee, F.H., ApJ, 398,476F (1992)

Fukugita, M., The Sloan Digital Sky Survey in proceedings of IAU, Kyoto, 1997, to be published in Highlights of Astronomy, vol. 11

Galaz G., de Lapparent V., 1998, A&A, 332, 459

Glazebrook, K., Offer, A.R., Deeley, K., 1998, ApJ, 492, 98

Gunn, J.E, Stryker, L.L., 1983, ApJ Supplement, 52,121

Gunn, J.E., Weinberg, D.H., in Wide Field Spectrsocopy and the Distant Universe, ed by S.J. Maddox and A. Aragón-Salamanca (World Scientific, Singapore, 1995)

Kennicutt, R.C., Jr., 1992, ApJ Supplement, 79, 2, 255

Leitherer, C., Fritze-von Alvensleben, U., Huchara, J. (eds.) 1996, From stars to galaxies; The impact of Stellar Physics on Galaxy Evolution, ASP Conf. Series., Vol. 98

Lejeune, T., Cuisinier, F., Buser, R., 1996, AAS CD-ROM Series, Vol. 7

Murtagh F., Heck A., 1987, Multivariate Data Analysis, Reidel, Dordrecht

Osterbrock D. E., 1989, Astrophysics of Gaseous Nebulae and Active Galactic Nuclei, Mill Valley, CA. University Science Books

Scalo J.M., 1986, Fund. Cosm. Phys. 11, 1

Sodré L. Jr., Cuevas H., 1997, MNRAS, 287, 137

Tinsley, B.M., 1980, Fundam. Cosmic Physics, 5, 287

Worthey,G., 1994, ApJ Supplement , 95, 1, 107

This paper has been produced using the Royal Astronomical Society/Blackwell Science LaTeX style file.